Title: A connexin 43 targeting peptide prevents blood vessel neointima formation

Running Title: CycliCx peptide disrupts neointima

Authors:, Mark C. Renton[1#], Meghan W. Sedovy[1,2#], Xinyan Leng[1], Farwah Iqbal[3], Melissa R. Leaf[3], Kailynn Roberts[1,2], Ramya C. Joshi[1], Arya Malek[1], Clare L. Dennison[1], Angela K Best[4], Paul D. Lampe[5], Joseph W. Baker[3,6], Mark Joseph[3,6], George S. Baillie[7], Brant E. Isakson[4,8] and Scott R. Johnstone[1,3,6,9*]

Affiliations:

[1] The Fralin Biomedical Research Institute at Virginia Tech Carilion, Center for Vascular and Heart Research, 4 Riverside Circle, Roanoke, Virginia, VA 24016 USA

[2] Translational Biology, Medicine, and Health Graduate Program, Virginia Tech, Blacksburg, VA 24061, USA

[3] Virginia Tech Carilion School of Medicine, Roanoke, VA 24016 USA

[4] Robert M. Berne Cardiovascular Research Center, University of Virginia School of Medicine, Virginia, VA 22908, USA

[5] Fred Hutchinson Cancer Research Center, Seattle, WA 98109 USA.

[6] Department of Surgery, Virginia Tech Carilion School of Medicine, Roanoke, VA 24016 USA

[7] School of Cardiovascular and Metabolic Health, University of Glasgow, Glasgow, UK G128QQ, UK

[8] Department of Molecular Physiology and Biophysics, University of Virginia School of Medicine, Virginia, VA 22908, USA

[9] Department of Biological Sciences, College of Science, Virginia Tech, Blacksburg, VA 24061, USA

Coauthors: Mark C. Renton and Meghan W. Sedovy share the position of first author.

* **Corresponding Author:**

Scott R. Johnstone, The Fralin Biomedical Research Institute at Virginia Tech Carilion, Roanoke, VA 24016, USA. Email: scottrj@vt.edu Phone: (+44) 540-526-2296

Conflict-of-Interest Statement:

The authors have declared no conflict of interest exists. Peptides generated and used in this manuscript are covered by patent #WO2021021716 (SRJ, BEI).

Abstract:

The gap junction protein connexin 43 (Cx43) is associated with human pathological vascular smooth muscle cell (SMC) proliferation and neointima formation. We previously identified mitogen-activated protein kinase (MAPK) phosphorylation of Cx43 results in binding with the cell cycle protein cyclin E, facilitating neointima formation in mice. However, the specific nature of these interactions and their relevance to human disease have not been elucidated. Using an *ex vivo* human saphenous vein model of neointima formation, we identified increased MAPK-phosphorylated Cx43 and cyclin E in explant tissues. We used peptide arrays to define a cyclin E-Cx43 binding region and generated 'CycliCx', a stearate-linked Cx43 phospho-mimetic peptide. In human coronary artery SMC, CycliCx inhibits platelet-derived growth factor-BB (PDGF-β)-induced changes in Cx43 trafficking and interactions with cyclin E, and stimulation of proliferation. RNAseq analysis identified CycliCx significantly inhibits PDGF-β-induced proliferative pathways in SMC by limiting PDGF-β-induced early G1/S phase cell cycle progression transcripts. Finally, we show CycliCx limits neointima formation in mice *in vivo* and in *ex vivo* human saphenous vein explants. Our data provide strong evidence for selective targeting of Cx43 as a viable therapeutic strategy for preventing neointimal formation in humans.

48 **Introduction:**

49 Atherosclerosis in the coronary artery narrows the vessel lumen, restricting arterial blood flow,
50 affecting more than 20.5 million Americans, making it the primary underlying cause of
51 cardiovascular disease[1]. Surgical interventions, such as coronary artery bypass and
52 percutaneous coronary interventions (angioplasty/stent placement), can be employed to
53 revascularize and alleviate symptoms and risks of coronary artery disease. Of those who undergo
54 surgical revascularization, 16.4% will experience a serious adverse event, including a heart attack
55 or death[2]. This highlights the need for novel therapeutics to enhance vessel patency following
56 revascularization surgeries.

57 The leading cause of long-term patency issues after coronary artery bypass grafting (CABG) or
58 percutaneous coronary intervention is neointimal hyperplasia[3], which occurs when vascular
59 smooth muscle cells (SMC) in the medial layer of arteries/ vascular conduits dedifferentiate, take
60 on a proliferative and migratory phenotype, and block the vessel intima[3]. Drug-eluting stents are
61 often used to limit neointimal growth, yet these stents use broad antiproliferative agents, which
62 delay vessel healing and necessitate the prolonged use of dual antiplatelet therapy, increasing
63 the risk of clinically significant bleeding[3-5]. As such, identifying mechanisms of neointima
64 development specific to SMC proliferation is essential in developing novel therapeutics.

65 Connexins form hexamers on the plasma membrane, which dock with connexin hexamers on
66 adjacent cells, forming gap junctions, facilitating cell-cell communication[6]. Increasing evidence
67 suggests connexins also regulate cell function in a gap junction-independent manner through
68 protein-protein interactions[7-14]. In SMC, altered Cx43 expression has been associated with
69 neointimal hyperplasia, but the specific role Cx43 plays remains unresolved, with conflicting
70 studies showing both increased and decreased proliferative states in response to altered Cx43
71 expression[15-19]. Additionally, decreased expression and gap junction signaling are associated with
72 both enhanced and delayed vascular disease progression[15,16,20-22].

73 Nuclear magnetic resonance analysis of the cytoplasmic Cx43 C-terminus reveals two α-helical
74 regions with a randomly coiled structure for the remaining length, forming a flexible protein primed
75 for phosphorylation and protein-protein interactions[23]. In addition, Cx43 contains a long
76 intracellular C-terminus with a high percentage of amino acids (a.a.) that can be post-
77 translationally modified[10,24,25]. Phosphorylation state influences the conformation of the Cx43 C-
78 terminus, altering the accessibility of other Cx43 phosphorylation sites and regulating the Cx43
79 protein-protein binding affinity[26]. Our previous study showed in response to platelet-derived
80 growth factor-BB (PDGF-β), Cx43 is phosphorylated by mitogen-activated protein kinases

81 (MAPK) at four of its C-terminal serines[24]. Phosphorylation by MAPK promotes Cx43 binding to
82 the cyclin E protein, which binds with CDK2 to promote G1/S phase cell cycle transition[24,27], and
83 results in SMC proliferation in mice[24]. Our previous data suggested disrupting Cx43-MAPK
84 activation does not compromise the viability of healthy SMC *in vivo,* making it a suitable target for
85 therapeutic intervention[24]. In transgenic Cx43-MAPK phosphorylation-null mice, Cyclin E-Cx43
86 interactions were inhibited, and ligation-induced carotid artery neointima was reduced[24]. Despite
87 this, the binding sites for Cx43 and cyclin E have not been elucidated.

88 In the present study, we aimed to define the importance of cyclin E-Cx43 interactions in human
89 vascular tissues during neointima formation, and hypothesized that disrupting cyclin E-Cx43
90 protein-protein interactions could prevent neointima formation. We developed models of *ex vivo*
91 human neointima formation using excess human saphenous veins intended for coronary artery
92 bypass grafts and show alterations in cyclin E and Cx43 protein expression and phosphorylation
93 during PDGF-β-induced SMC proliferation. We used peptide array techniques to define a 14 a.a.,
94 phospho-dependent cyclin E binding site on Cx43 and developed a stearate-linked linear peptide
95 ('CycliCx') to disrupt cyclin E-Cx43 interactions. *In vitro* testing demonstrated CycliCx inhibits
96 PDGF-β-induced changes in Cx43 localization and phosphorylation state, limits cyclin E-Cx43
97 interactions, and reduces human SMC proliferation. Transcriptomics data highlighted the CycliCx
98 peptide disrupts PDGF-β-induced gene pathways regulating G1/S phase cell cycle progression
99 in cultured human SMC. Importantly, our data show CycliCx is a potent inhibitor of neointima in
100 mouse and human models. This study is the first to demonstrate specific binding domains for
101 cyclin E-Cx43, show relevance in human disease, and identify a specific molecule targeted to
102 SMC that limits neointima formation.

Results

A human saphenous vein model of neointima formation shows Cx43 MAPK-phosphorylation in new intima cells. Previous *ex vivo* models of human saphenous vein neointima developed by George et al.[28,29] demonstrated high serum levels promote SMC proliferation and migration to the intimal surface of tissue explants, forming a "new intima" on the surface of the explants. We aimed to adapt this model to examine the effects of PDGF-β-induced proliferation using low serum media (**Figure 1A**). Human saphenous vein tissue explants underwent no treatment (NT; no PDGF-β) or 14-day treatment (PDGF-β, 50 ng/mL). Histological staining demonstrated an increase in cell layers at the surface of the explants in PDGF-β-treated tissue (**Figure 1B, Supplemental Figure 1**). The appearance of the cells is consistent with the new intima in previously published models for *ex vivo* HSV intimal growth[28,29]. Immunofluorescent staining demonstrated cells in the upper layers of the tissue are transgelin (TGLN) positive SMC, with significant increases in TGLN staining in PDGF-β-treated tissues (**Figure 1B, Supplemental Figure 2**). Staining also identified high levels of expression for total Cx43 and cyclin E within these cells, and antibodies specific to MAPK-phosphorylated sites on Cx43[24] highlight PDGF-β promotes Cx43-MAPK phosphorylation in human tissues (**Figure 1B, Supplemental Figures 3-5)**.

Identification of a binding region between Cx43 and cyclin E and development of the CycliCx peptide. Our previously published data suggest phosphorylation at Cx43-MAPK C-terminal serines (S) regulates protein interactions between cyclin E and the Cx43 C-terminus[24]. However, specific sites of interaction are unknown, and structural modeling of Cx43 is limited. Therefore, we used a peptide array approach to define the critical binding sites of the Cx43 C-terminus required for binding with cyclin E. Peptide arrays of the full Cx43 C-terminus (a.a. 236-382) were designed with 25 a.a. peptide sequences arranged sequentially, with a five a.a. overlap between each sequence (**Figure 2A**). Arrays were arranged to test a requirement of the Cx43-MAPK serines located at S255/S262/S279/S282 (MK4) on Cx43, using either: non-mutated serines ($Cx43^{wt}$, non-phosphorylated state), serine to alanine (A) mutations ($Cx43^{MK4A}$, non-phosphorylatable state), serine to aspartate (D) mutations ($Cx43^{MK4D}$, phosphorylated state mimic), or native phosphoserines (pS) ($Cx43^{MK4pS}$, phosphorylated state). The full-length cyclin E protein was synthesized as we previously described[24] (**Figure 2B**). Isolated cyclin E proteins were incubated with Cx43 peptide arrays, and binding was detected using antibodies targeting cyclin E (**Figure 2C-D**). Initial peptide arrays identified three potential binding regions in each of the $Cx43^{MK4D}$ and $Cx43^{MK4pS}$ sequences (**Figure 2C-D**). Given consensus between D/pS binding

136 regions, we focused on a.a. 236-301, which were divided into three separate, but overlapping, 25
137 a.a. peptide sequences: Seq1 a.a. 235-260 (gray), Seq 2 a.a. 254-279 (green), Seq 3 a.a. 276-
138 301 (black) (**Figure 2 E-F**). To test the requirement of single a.a., we prepared arrays using
139 alanine substitutions along the length of each sequence, incorporating phosphorylation of Cx43-
140 MAPK serines where they occurred. Our data indicate consistent binding when phosphorylation
141 was present in Seq 1 and Seq 2, but no evidence of binding in Seq 3 (**Figure 2G**). Further, single
142 a.a. substitutions did not significantly impact overall binding in Seq 1-2 (**Supplemental Figure**
143 **6A**).

144 Using a truncation mutation peptide array approach, which reduces the sequence length by a
145 single a.a. at a time, we tested regions of interest within the identified short region
146 GVKDRVKGRSD (Peptide-1, 11 a.a.) and longer region LDPSKDCGDPKYAYFNGCSSPT
147 (Peptide-2, 22 a.a.) that showed cyclin E binding (**Supplemental Figure 6B-C**). We synthesized
148 peptides for these sequences, conjugated with an N-terminal stearyl group to aid in peptide
149 cellular internalization. Peptides (30 μM) were incubated with cell cycle-stalled primary human
150 coronary artery smooth muscle cells (CASMC) treated with PDGF-β (50 ng/mL) to promote
151 proliferation. We used 5-ethynyl 2´-deoxyuridine (EDU) to label newly synthesized DNA and
152 measured proliferation by flow cytometry. At 48 hours, PDGF-β increased proliferation in CASMC,
153 which was reduced by Peptide 2 without notable cell loss (**Supplemental Figure 6D**). However,
154 Peptide 1 treatment resulted in significant cell loss and was not tested further (**Supplemental**
155 **Figure 6D**).

156 Peptide arrays indicated a minimum binding sequence within Peptide 2, between a.a. 254-268,
157 but a loss of signal after removal of Tyrosine 267 (**Figure 2H, Supplemental Figure 6C**). Based
158 on this, we created 'CycliCx', a 14 a.a. sequence, LDPSKDCGDPKYAY, which showed cyclin E-
159 Cx43 binding. We also made a control off-target peptide (OT-peptide), a 15 a.a. sequence,
160 AYFNGCSSPTAPLDP, which represents the immediately adjacent a.a. sequence unable to bind
161 cyclin E. Both peptides were synthesized with an N-terminal stearate to promote cell entry, giving
162 a final design of stearate-LDPSKDCGDPKYAY (CycliCx), and stearate-AYFNGCSSPTAPLDP
163 (OT peptide), which was used as a control treatment throughout this study (**Fig 2H-I**). Because
164 the CycliCx sequence was initially based on the mouse Cx43 sequence, we created a humanized
165 CycliCx peptide, stearate-LDPAKDCGDQKYAY, for testing (**Fig 2I**). In testing, we saw no
166 differences between mouse and human CycliCx peptides in their effects on cells (not shown). The
167 human CycliCx peptide was used for all future experiments. The two peptides have approximately
168 the same molecular weight and charge. The CycliCx peptide has a sequence predicted MW of

169 1571 kDa, (1853.22 kDa with stearate group) and a charge of -1, and the OT peptide has a
170 predicted MW of 1586 kDa (1806.01 kDa with stearate group) and a charge of -1 (**Supplemental**
171 **Figure 6E-F**).

172 **CycliCx peptide alters Cx43 cellular functions in human CASMC.** Our previous data showed
173 PDGF-β-induced ERK phosphorylation is a key factor in regulating cyclin E-Cx43 protein
174 interactions in mouse primary SMC[24]. To assess ERK activation, human CASMC were treated
175 with PDGF-β (50 ng/mL) to induce proliferation. Treatment with PDGF-β significantly upregulated
176 ERK Threonine 202/Tyrosine 204 phosphorylation (pERK) in CASMC (**Figure 3A, Supplemental**
177 **Figure 7**). Treatment of CASMC with either CycliCx or OT-peptide (30 μM each) did not
178 significantly alter levels of PDGF-β-induced pERK in CASMC (**Figure 3A, Supplemental Figure**
179 **7**). In addition, total Cx43 expression was not affected by PDGF-β in CASMC. However, CycliCx
180 altered Cx43 western blot protein banding (loss of upper phosphorylated bands), while OT-
181 peptide had no effect (**Figure 3B, Supplemental Figure 8**). Based on previous reports of
182 phosphorylation states present in each migrating band, we assessed Cx43 protein kinase-C
183 (PKC) phosphorylation at Cx43-S368 (Cx43-pS368). Our data highlight CycliCx significantly
184 increases phosphorylation at Cx43-S368 in CASMC (**Figure 3B, Supplemental Figure 8**). While
185 most experiments in cells were performed at 16 hours, we found CycliCx produced alterations in
186 Cx43-S368 phosphorylation as early as 3 hours (**Supplemental Figure 9**).

187 To assess Cx43 expression and localization, we performed immunofluorescence of cultured
188 CASMC and identified punctate staining characteristic of Cx43, which was not significantly altered
189 by treatment with PDGF-β or PDGF-β+OT peptide (**Figure 3C, Supplemental Figure 10**). In
190 PDGF-β+CycliCx-treated cells, Cx43 GJ punctates were significantly reduced, and staining
191 appeared more diffuse (**Figure 3C, Supplemental Figure 10**). Membrane biotinylation
192 experiments demonstrated PDGF-β and PDGF-β+OT peptide treatments reduced Cx43
193 expression at the plasma membrane. CycliCx inhibited the PDGF-β-induced removal of Cx43
194 from the plasma membrane (**Figure 3D, Supplemental Figure 11**). To test whether CycliCx
195 altered gap junction signaling, we performed scrape-loading dye-transfer assays using the gap
196 junction-permeable lucifer yellow dye. We found CycliCx inhibited Cx43 dye transfer through gap
197 junctions compared to controls (**Figure 3E, Supplemental Figure 12**). Finally, we tested if
198 CycliCx could inhibit interactions between Cx43 and cyclin E. Co-immunoprecipitation assays
199 demonstrated PDGF-β treatment increased cyclin E-Cx43 complex formation in human CASMC,
200 which was significantly reduced by treatment with CycliCx (**Figure 3F, Supplemental Figure 13**).

201 **CycliCx peptide inhibits PDGF-β-induced proliferation by blocking G1/S phase cell cycle**
202 **transition.** To test if CycliCx alters the proliferation of SMC in a human model, we assessed
203 PDGF-β-induced proliferation in CASMC by EDU flow cytometry. We found PDGF-β significantly
204 upregulated CASMC proliferation, which was inhibited by treatment with CycliCx. (**Figure 4A-C**,
205 **Supplemental Figure 14**). Bulk RNA sequencing of CASMC revealed PDGF-β+CycliCx altered
206 the transcript expression of more genes than PDGF-β+OT peptide when compared with PDGF-β
207 alone (**Figures 4D-E**). Pathway enrichment analysis using the Gene Ontology (GO) database
208 demonstrated a significant upregulation of pathways involved in cell cycle progression and mitotic
209 nuclear division in PDGF-β-treated compared to control CASMC, indicating CASMC
210 differentiation into a pro-proliferative phenotype (**Figure 4F**). The addition of the CycliCx peptide
211 resulted in significantly decreased enrichment of these same proliferative pathways when
212 compared to PDGF-β treatment alone and to PDGF-β+OT peptide-treated CASMC (**Figure 4F,**
213 **Supplemental Figure 16**).

214 Furthermore, CycliCx treatment significantly blunted the PDGF-β-induced transcript expression
215 of large arrays of genes involved in 'cell cycle G1/S phase transition' (GO:0000082; **Figure 4G**),
216 'cell cycle G2/M phase transition' (GO:0044839), and 'mitotic nuclear division' (GO:0140014;
217 **Supplemental Figure 16**). Importantly, PDGF-β+OT peptide treatment did not significantly blunt
218 the PDGF-β-induced expression of these genes. We next interrogated the expression of key
219 regulatory genes at each phase of the cell cycle (**Figure 4G**; **Supplemental Figure 17**) and found
220 CycliCx treatment had no effect on the PDGF-β-induced expression of Ccnd1 (Cyclin D1) and
221 Cdk4, which regulate early G1 progression, but partially blunted Cdk6 and Cdkn2c (p18)
222 expression (**Supplemental Figure 17A**). Although CycliCx impairs binding of Cyclin E, it had no
223 effect on Ccne1 (cyclin E1) gene expression (**Figure 4H)**. However, CycliCx significantly blunted
224 the PDGF-β-induced increase in the expression of G1/S phase transition promoters Cdk2 and
225 E2f1 and partially reversed the PDGF-β-induced decrease in expression of G1/S phase transition
226 inhibitors Tp53 (p53) and Cdkn1a (p21) (**Figure 4H**; **Supplemental Figure 17B**). Finally, we
227 assessed late G2/M phase regulatory genes and found CycliCx inhibited the PDGF-β-induced
228 increase in Ccna2 (Cyclin A2) and Cdk1, while OT peptide treatment had no effect (**Figure 4H**;
229 **Supplemental Figure 17C**). Last, CycliCx did not alter the expression of Cx43 (**Figure 4H**), other
230 canonical PDGF-β transcription targets such as Timp1 (**Figure 4H**), Timp3, and Il1b, or the
231 downstream effector kinases Mapk3 (Erk1) and Mapk1 (Erk2; **Supplemental Figure 18B**). Last,
232 smooth muscle contractile markers were decreased by treatment with PDGF-β, but treatments
233 with CycliCx or OT peptide did not prevent this PDGF-β-induced transcriptional change
234 (**Supplemental Figure 19**).

235 **CycliCx peptide disrupts neointima formation in mice and human blood vessels.** To test
236 CycliCx *in vivo*, we performed carotid ligation surgeries in mice and applied peptides mixed in
237 Pluronic gel directly to the outside of carotids (**Figure 6A**). We found significant neointima
238 formation in pluronic controls and OT peptide-treated mice compared with sham ligation mice
239 (**Figure 6A**). Treatment with CycliCx peptide significantly inhibited ligation-induced neointima in
240 mice and was not significantly different from sham control mice (**Figure 6A, Supplemental**
241 **Figure 20)**. We found no sex differences in mice in terms of neointima formation or the effect of
242 the peptide, and data shown represent both male and female mice (**Supplemental Figure 20**).
243 We then tested the effect of CycliCx in PDGF-β-induced neointima formation in *ex vivo* human
244 saphenous veins. As shown in **Figure 1B and Supplemental Figures 1-5**, PDGF-β promotes
245 the formation of SMC-derived new intima regions at the surface of tissue explants compared to
246 NT. This is significantly increased when compared with no treatment (NT) at 14 days and is
247 unaffected by OT-peptide treatments (**Figure 6B, Supplemental Figures 1-5)**. In *ex vivo* human
248 saphenous veins, CycliCx significantly reduces the presence of SMC in the intimal region of
249 explants, suggesting inhibition of neointima formation (**Figure 6B, Supplemental Figures 1-5)**.

250 **Discussion**

251 Targeted therapies to address the mechanisms of neointima formation are needed to reduce the
252 risk of stent/bypass failure. Our previously published data identified phosphorylation of Cx43 at
253 its C-terminus MAPK residues regulates SMC proliferation and neointima formation in mouse
254 models[24]. This control of SMC proliferation is dependent on interactions between the Cx43 C-
255 terminus and cell cycle-regulating protein cyclin E[24]. In the present study, we defined for the first
256 time the binding region of cyclin E on Cx43 and demonstrated MAPK phosphorylation sites within
257 this binding region are required for direct cyclin E-Cx43 interactions. We developed the CycliCx
258 peptide, which mimics a short 14 a.a phosphorylated region of the Cx43 C-terminus within the
259 MAPK region, and was designed to inhibit cyclin E-Cx43 binding. Our data highlight CycliCx alters
260 Cx43 localization, signaling, and trafficking while limiting cyclin E binding with Cx43. Using a
261 transcriptomic approach, we found CycliCx significantly blunts PDGF-β-induced cell cycle
262 progression, leading to reduced proliferation in cultured human CASMC. Finally, we showed
263 CycliCx significantly alters neointima formation in models of disease in mouse and human tissues.
264 This work establishes critical binding sites on Cx43 required for SMC proliferation and identifies
265 Cx43 as a viable therapeutic target for the prevention of human neointima formation.

266 Current strategies for mitigating neointima formation after stenting procedures primarily include
267 the use of non-cell-specific drugs such as the Rapamycin analogs, Everolimus and Zotarolimus.
268 These drugs work by targeting mTOR signaling, a pathway essential for protein, nucleotide, and
269 lipid synthesis, ultimately regulating cell growth and division[30]. Although mTOR inhibitors can stop
270 the pathological proliferation and migration of SMC, which form neointima, they present a risk to
271 other cell types in the vasculature, particularly endothelial cells that protect the vessel from platelet
272 aggregation and ultimately thrombus formation[4]. Our recent investigation revealed significant
273 endothelial damage caused by standard preservation techniques during coronary bypass surgery,
274 and highlighted the need for endothelial healing[31]. Targeting cyclin E-Cx43 interactions disrupts
275 a key signal required for pathological SMC growth without impacting cell viability or global mTOR
276 signaling. As such, this is a promising strategy for targeting neointima formation/restenosis
277 without impacting healthy cellular healing functions and adversely impacting patient health.

278 Emerging research reveals Cx43 proteins can act independent of forming cell-cell gap junction
279 channels to control cellular functions[7-13]. We previously described Cx43 interacts with the cell
280 cycle control protein cyclin E in mouse SMC *in vitro* and *in vivo*. Cyclin E tightly controls G1/S
281 phase cell cycle transition, which is critical for pathological SMC proliferation[27,32]. Our data in
282 human saphenous vein explants showed both Cx43 and cyclin E are expressed in the new intima

283 layers after PDGF-β stimulation, suggesting a role for Cx43 in the SMC proliferation in these
284 tissues. Given our previous evidence that blocking these interactions is important in mouse
285 neointima formation, we set out to define the role of cyclinE-Cx43 interactions in human neointima
286 and SMC proliferation.

287 This is the first study to comprehensively define the location of cyclin E-Cx43 binding. We
288 identified two regions on the Cx43 C-terminus with consistent cyclin E binding activity and used
289 these to generate Cx43 mimetic peptides. The first region, used to generate peptide-1, spans
290 Cx43 a.a. 235-245, which does not encompass any reported Cx43-MAPK phosphorylation sites.
291 This peptide is highly similar to the Cx43 mimetic peptide juxtamembrane 2 (JM2)[33]. The JM2
292 peptide sequence is designed to cover the binding region between Cx43 and microtubule subunit
293 β-tubulin[33]. JM2 enhances the Cx43 β-tubulin interactions, reduces Cx43 trafficking to the plasma
294 membrane, and reduces Cx43 hemichannel ATP release[33,34]. In our *in vitro* model of PDGF-β-
295 induced CASMC proliferation, the overlapping peptide 1 resulted in cell loss, and further testing
296 of this peptide was not performed, as our goal is to limit CASMC from entering a proliferative
297 phenotype while maintaining vessel health. This is in line with previous work in 4T1 tumor cells,
298 in which JM2 was found to induce ROS-mediated apoptosis by disrupting mitochondrial
299 trafficking[35]. However, no JM2 cytotoxicity was reported in healthy cultured human microvascular
300 endothelial cells[33]. Conflicting cellular responses to the JM2/peptide 1 sequences could arise from
301 differences in cell types, with CASMC more susceptible to cell loss than the endothelium from this
302 peptide sequence. Duration of treatment and dose may also be responsible for the differential
303 effects reported.

304 The second cyclin E-Cx43 binding region, used to generate peptide 2 and the final CycliCx
305 peptide, spans Cx43 a.a. 254-275, with phosphomimetic aspartate mutations at the known Cx43-
306 MAPK phosphorylation sites, S255 and S262. Cyclin-dependent kinase 1 (CDK1) and ERK5 are
307 implicated in the phosphorylation of Cx43 at one or both of the S255 and S262 sites[36-38], which
308 correlate with gap junction internalization and cell division[24,36-39]. To include an appropriate control
309 condition when testing the CycliCx peptide, we developed the OT peptide based on the sequence
310 immediately adjacent to CycliCx (Cx43 a.a. 266-280). The OT peptide contains the known Cx43-
311 MAPK phosphorylation site Cx43 S279 (but not the S282 site), and in line with the CycliCx
312 peptide, the OT peptide contains a phosphomimetic aspartate at its corresponding residue and
313 an identical N-terminal stearate group. The OT peptide sequence was selected as a control due
314 to its proximity to CycliCx and lack of cyclin E binding activity. The OT peptide is similar to the first
315 15 a.a. of the 18 a.a. TAT-Cx43266-283 peptide published by Gangoso et al., with the exception

316 of the a.a. 279 serine to aspartate mutation[7,40]. TAT-Cx43266-283 is a Cx43 mimetic based on
317 the cSRC binding domain. cSRC perpetuates cell proliferation in some cancers, and evidence
318 suggests binding with Cx43 inactivates cSRC and limits cancer growth. It is thought TAT-
319 Cx43266-283 binds cSRC directly, mimicking the effect of full-length Cx43 and limiting
320 glioblastoma growth in culture and *in vivo*[7,40]. In the present study, the OT peptide did not inhibit
321 SMC proliferation or neointima formation. Due to the similarity between TAT-Cx43266-283 and
322 our OT peptide, it is possible our OT peptide is lacking critical a.a. for cSRC binding, the aspartate
323 mutation within the OT peptide prevents cSRC binding, or cSRC does not play a significant role
324 in injury-induced proliferation in SMC.

325 Proposed mechanisms of action for previously published Cx43 mimetic peptides include binding
326 between the Cx43 mimetic and a physically interacting protein, or direct binding between the Cx43
327 mimetic and Cx43 itself[7,40,41]. Our peptide array data demonstrate sequences for CycliCx and the
328 cyclin E protein can bind directly. Although we do not present direct evidence of CycliCx-Cx43
329 interactions, CycliCx induced a shift in Cx43 molecular weight attributable to an increase in Cx43-
330 pS368, a known PKC phosphorylation site. Cx43-pS368 phosphorylation is associated with
331 control over gap junction open/closed states and has been observed with other Cx43 mimetic
332 peptides, a phenomenon we summarized in our previously published review[42]. For example, the
333 Cx43 mimetic peptide αCT1, developed by the Gourdie lab to disrupt Cx43/ZO-1 interactions,
334 binds directly to the Cx43 C-terminus, causing an increase in Cx43-PKC phosphorylation[41].
335 Mutating αCT1 to interact only with ZO-1 and not directly with Cx43 did not produce increases in
336 Cx43-pS368, indicating direct Cx43 binding is required for αCT1-induced Cx43-pS368[41]. As
337 CycliCx induces a similar phosphorylation shift, it is possible CycliCx is also capable of directly
338 binding the Cx43 protein.

339 Cyclin E exerts control over the cell cycle via binding with its kinase CDK2. Although the complete
340 mechanism of action of cyclin E-CDK2 is uncertain, it is known this complex translocates from the
341 cytoplasm to the cell nucleus to phosphorylate the retinoblastoma protein and exert its effect on
342 cell division[43-46]. In our previous studies, cyclin E-Cx43 complexes are initially present in the cell
343 membrane but bind Cx43 and are removed after prolonged PDGF-β treatment, demonstrating
344 Cx43 can accompany cyclin E-CDK2 during translocation[24]. In the present study, CycliCx
345 treatment retained Cx43 at the cell membrane after PDGF-β treatment, likely attributable to the
346 shift toward Cx43-pS368 phosphorylation, which is associated with stabilizing Cx43 at the
347 membrane[47,48]. Therefore, it is possible Cx43 is required to chaperone cyclin E to the cell nucleus

348 to progress the cell cycle and induce proliferation, and disrupting the cyclin E-Cx43 complex
349 interaction and trafficking prevents this.

350 In line with this, our transcriptomic data suggest CycliCx treatment blunts the PDGF-β-induced
351 increase in transcript expression of critical cell cycle promoter genes downstream of the cyclin E-
352 CDK2 complex. Cyclin E-CDK2 primarily regulates the G1/S phase transition of the cell cycle[27].
353 Indeed, there was little change in the expression of genes involved in the regulation of the early
354 G1 phase of cell cycle progression with CycliCx treatment, while CycliCx significantly blunted the
355 PDGF-β-induced regulation of G1/S phase transition and subsequent G2/M phase transition and
356 M phase genes. This suggests CycliCx targets cyclin E to arrest the cell cycle during the G1/S
357 phase transition.

358 In addition to halting pathological SMC proliferation and neointima formation, it is important to
359 examine potential off-target effects of the CycliCx peptide. We found many PDGF-β downstream
360 transcription targets unrelated to cell cycle, such as tissue inhibitors of metalloproteases (TIMPs)
361 and interleukins, were not affected by the CycliCx peptide. Our investigation also revealed a
362 reduction in gap junction communication following CycliCx treatment. This may be attributable to
363 the observed increase in Cx43-pS368, which is associated with gap junction closure[49,50].
364 Interestingly, PDGF-β also induced gene expression of Cx40, which was reduced after treatment
365 with CycliCx. Together, these data demonstrate CycliCx treatment specifically inhibits PDGF-β-
366 induced pathological SMC cell cycle progression without significant disruption to other cell
367 signaling pathways.

368 A caveat to this study is the use of human veins over arteries in testing CycliCx treatment in
369 human tissues. In modern clinical practice, the internal mammary or radial arteries are preferred
370 for coronary bypass surgeries over the saphenous vein due to lower levels of neointima
371 formation[51-53]. Even so, the saphenous vein is still used more often than any other vessel for
372 coronary bypass when additional bypass conduits are required[54]. As such, testing CycliCx in
373 venous tissue is highly relevant to surgical practice. Currently, we are unable to trace the half-life
374 of the CycliCx peptide due to a lack of available antibodies to CycliCx and the mechanism of
375 synthesizing the peptide. The CycliCx peptide is synthesized with an N-terminal stearate group,
376 limiting our ability to add a reporter such as GFP to the C-terminus. Attempts to add 6xHis tags
377 to the peptide resulted in insoluble peptides and were not viable for testing (not shown). However,
378 our data show clear effects *in vivo* in mice at 14 days, and our *in vitro* studies show CycliCx effects
379 appear around 3 hours and remain at >16 hours, suggesting a peptide with good stability,
380 although this remains to be fully elucidated. Our data also shows CycliCx limits gap junction

381 signaling; thus, we are unable to distinguish gap junction and connexin-mediated effects directly
382 in this study. However, our previous study found that Cx43-gap junction signaling did not play a
383 significant role in PDGF-β-induced SMC proliferation in mice[24]. The CycliCx peptide may therefore
384 also act as a promising tool for the specific regulation of gap junction signaling, which is not
385 currently available.

386 In conclusion, we show that targeting Cx43 and cyclin E interactions with the novel Cx43 mimetic
387 peptide CycliCx limits SMC proliferation and neointima formation in mice and human tissue. The
388 findings from this study highlight new pathways important in neointima formation, which could be
389 targeted to improve patency in human revascularization strategies. While our study focuses on
390 pathological proliferation of SMC in blood vessels, future research should test whether CycliCx
391 could be utilized in other diseases of pathological proliferation for which Cx43 has been implicated
392 in[55].

393 **Methods**

394 **Sex as a biological variable:** Male and female mice were used to assess sex as a biological
395 variable in animal studies. Our data do not show differences in cell pathology or neointima
396 formation in male vs female mice, and the results report combined data for both male and female
397 mice. The sex of the individual mice is indicated in **Supplemental Figure 20**.

398 **Key Resources:** Reagents, materials, and antibodies are all listed in **Supplemental Table 1**

399 ***Ex vivo* human saphenous vein model of neointima formation:** We adapted a previously
400 described *ex vivo* model of human saphenous vein neointima formation developed by George et
401 al.[28,29]. At the end of surgical procedures for coronary artery bypass graft, excess, normally
402 discarded saphenous vein tissue was collected. De-identified specimens from Carilion Clinic
403 cardiovascular patients were processed within 1 hr of the end of surgery. Tissues greater than 2
404 inches in length, free from visible valves and branch regions, were used in the study. Tissues
405 were placed into a container of harvest media (20 mM HEPES-buffered RPMI-1640, 0.225 mg/mL
406 papaverine hydrochloride, 5 µg/ml amphotericin B, 20 IU/mL sodium heparin). Samples were
407 transferred to a wash media (20 mM HEPES Buffered RPMI-1640 with 2 mM L-Glut, 8 µg/mL
408 gentamicin, 1 IU/mL penicillin, and 1 µg/mL streptomycin). Tissues were cut into four consecutive
409 explant sections and pinned on 6-well plates containing Sylgard 184 elastomer (**Figure 1**).
410 Explants were maintained in a low-serum media (bicarbonate buffered RPMI-1640, 2 mM L-Glut,
411 8 ug/mL gentamicin, 1 IU/mL penicillin, 1 µg/mL streptomycin, and 2% FBS). The four treatment
412 groups corresponding to four sections were: 1) no treatment; 2) PDGF-β (50 ng/mL, Millipore #01-
413 305); 3) PDGF-β (50 ng/mL) plus OT peptide (30 µM); and 4) PDGF-β (50 ng/mL) plus CycliCx
414 peptide (30 µM). Media were changed each day for 14 days. At the end of the experiments, tissue
415 explants were fixed *in situ* in 4% PFA at 4°C overnight. To preserve integrity, tissues were
416 encapsulated in 3% agarose before tissue processing and paraffin embedding by the FBRI
417 Histology Core.

418 **Cx43 peptide arrays for cyclin E binding:** SPOT synthesis of peptides and overlay experiments
419 were carried out as described[56]. Arrays were used as an n=1 in most cases. However, each spot
420 represents unique, but overlapping sequences, which are replicated multiple times across multiple
421 blots. Full-length cyclin E-GST protein was synthesized as previously described by us[24]. Cyclin
422 E-GST proteins for arrays were isolated using anti-GST beads, spin concentrated (Amicon, 10K
423 MWCO, Millipore #UFC901008), and buffer exchanged to PBS 125 mM NaCl, pH 6.5 on PD10
424 columns (Millipore #GE17-0851-01). Peptide arrays were initially bathed in 100% ethanol,
425 equilibrated in PBS-Tween (PBST, 125 mM NaCl, 0.1% tween, pH 6.5) for 10 min, then blocked

426 in PBST-5% block (PBST with 5% milk) at room temperature for 2 hr. Arrays were washed in
427 PBST, then incubated with cyclin E proteins (2.86 mg/mL) in PBST-1% block (1% Milk). Binding
428 on arrays was detected using cyclin E primary antibodies in PBST-1% block, followed by
429 secondary detection using rabbit HRP (Thermo Fisher #31458) in PBS-T-1% block for 1 hr at
430 room temp, then developed by chemiluminescent substrate (SuperSignal, Thermo Fisher #
431 34579) on x-ray film in a dark room. Developed films were scanned for image analysis (cyclin E,
432 Odyssey, LiCor). Arrays were imaged using UV to visualize total peptides (Odyssey, LiCor).
433 Sequences for the truncation mutation array can be found in **Supplemental List 1.**
434 **Peptides:** Peptides used in the studies were designed based on the peptide array minimal binding
435 sequences shown in **Figure 2**. Peptides were synthesized with an N-terminal stearate group to
436 improve cellular uptake[57]. Peptide final sequences used in the study are CycliCx: stearate-
437 LDPSKDCGDPKYAY and Off-Target (OT) peptide: stearate-AYFNGCSSPTAPLDP. Peptide
438 properties are described in **Supplemental Figure 6**. Patent #WO2021021716: "Compositions
439 and methods for inhibiting neointimal formation" covers the discovery and use of peptide (CycliCx)
440 and control peptides. Peptides were commercially synthesized (ThermoFisher custom peptide
441 synthesis services) to >80% purity (**Supplemental Figure 6F**). Peptides were reconstituted at
442 room temperature in sterile PBS (for cell culture) or saline (for *in vivo*) to a concentration of 2 mM
443 and stored at -80°C for use. Peptides used in cell culture and explant culture experiments were
444 prepared to a final concentration of 30 μM in media. Peptides for *in vivo* applications in mice were
445 prepared to a concentration of 200 μM in a Pluronic gel (35% final concentration), with 50 μL of
446 the Pluronic gel applied around the ligated carotids.

447 **Animals:** All mice were cared for under the provisions of the Virginia Tech Animal Care and Use
448 Committee and followed the National Institute of Health guidelines for the care and use of
449 laboratory animals. All studies were performed in C57BL6/J mice; strain number #000664,
450 purchased from Jackson Labs. Mice were bred in-house and used between 12-14 weeks of age.

451 **Carotid ligations and carotid Pluronic gel applications in mice:** A 50% Pluronic gel stock was
452 made by adding 3 g of Pluronic powder to 3 mL of ice-cold sterile saline and mixing under cold
453 conditions until dissolved. Pluronic gels were sterilized by autoclaving. For surgeries, Pluronic
454 stocks (50%) were mixed with sterile saline or with peptides in sterile saline to achieve a final
455 concentration of 35% Pluronic. Samples were maintained on ice to maintain a liquid form.
456 Permanent 14-day carotid ligations were used to promote neointima in mice, as we previously
457 described[24]. Mice were, anesthetized using isoflurane, placed on a surgically sterile heating pad
458 with isoflurane, and the neck area cleared of hair and sterilized. Mice received analgesic (Ethiqa

459 0.5 mL) proximal to the surgical site. An incision was made in the neckline of the mice, carotid
460 exposed, and a 6/0 suture was secured to the carotid immediately before the bifurcation. In sham
461 control mice, a 6/0 suture was passed under the exposed carotid and then removed. In ligated
462 and sham mice, carotids were elevated, and cold Pluronic gel (50 µL) was applied evenly around
463 the carotid using a positive displacement pipette. Carotids were held in place for around 10
464 seconds until the Pluronic gel solidified (as we previously described)[58]. The surgical site was then
465 closed, and the skin sutured, followed by post-operative recovery. Comparisons were made to
466 surgical controls (sham) and OT peptide controls.

467 **Cell culture:** Primary human CASMC were sourced from American Type Culture Collection
468 (ATCC, #PCS-100-02), ThermoFisher (#C0175C) and Lonza (#CC-2583). Initial stocks of cells
469 were thawed and maintained in vascular smooth muscle cell basal media (ThermoFisher #M231-
470 500) containing smooth muscle growth serum (SMGS, ThermoFisher # S00725). Cells were
471 maintained between 70-90% confluency in culture for up to 16 cell divisions. For experiments,
472 $5x10^4$ CASMC per mL were plated in each well of a six-well plate. CASMC were serum starved
473 to stall cell cycle by washing in PBS and then incubating with vascular smooth muscle cell basal
474 media containing 2% FBS for 72 hr prior to treatments. Media were changed every 48 hours.
475 Stalled CASMC were induced with PDGF-β (50 ng/mL) and harvested at 16 hr for western blot or
476 48 hr for flow cytometry of proliferation. For peptide treatments, cells were treated simultaneously
477 with PDGF-β (50 ng/mL) and peptide (30 µM).

478 **Flow cytometry:** For studies of proliferation, CASMC were treated with 5-ethynyl-2'deoxyuridine
479 (EDU, Thermo Fisher, #C10425) at the same time as PDGF-β and peptide treatments. At the end
480 of experiments, CASMC were trypsinized, centrifuged (700 rpm, 5 min), then resuspended in 0.5
481 mL PBS. Cells were fixed by adding 70% ethanol while vortexing. EDU detection was performed
482 as per the manufacturer's instructions. Flow cytometry data were collected using a BD Accuri C6
483 flow cytometer, and data analyzed using FlowJo software. Proliferation was calculated as a
484 percentage of EDU-positive cells to total cells.

485 **Immunofluorescence:** Tissues fixed in 4% PFA were embedded in paraffin and sectioned.
486 Antigen retrieval was performed (Universal R, antigen retrieval solution, Electron Microscopy
487 Solutions) on deparaffined slides containing tissue sections and tissues blocked in a solution of
488 PBS, 0.1% NP-40 substitute, 1% BSA, where required, BSA was replace with 5% anti-goat serum.
489 Primary antibody incubations were performed overnight at 4°C, samples washed, and secondary
490 antibodies applied.

491 **Imaging and analysis:** Histological imaging was completed on a Nikon Ci-L histology microscope
492 using tile scan/ Z-stack functions. Data for the quantification of neointima was performed by a
493 researcher blinded to sample identification. All immunofluorescent images were captured using
494 Nikon NIE confocal microscope (A1, with resonance scanning). Single images, maximum intensity
495 Z-stack projection, along with tile scanning, were used to visualize samples. All quantitative
496 analysis was performed using NIS Elements Advanced Research software (Nikon). Examples of
497 NIE image processing tool use are shown in **Supplemental Figures 2 and 12**. To analyze new
498 intima in TGLN-stained tissues, a line (16pt) was drawn at the luminal edge of the tissues using
499 NIE software using the signal intensity tool. Background signal was set for individual images
500 based on tissue autofluorescence, and the area under the curve (AUC) for the TGLN signal was
501 divided by the length of the tissue. 5-6 images were taken across each tissue, and the AUC was
502 averaged for these values. Representative patient TGLN images used for analysis are shown in
503 **Supplemental Figure 2**. For each HSV experiment, consecutive tissue samples are used, and a
504 fold change to the individual patient NT sample TGLN signal was made to calculate differences.

505 **Scrape load dye transfer (SLDT) assays:** Serum-starved CASMC were treated with PDGF-β
506 and peptides for 16 hr. Cells were washed in PBS with calcium and magnesium, and scratch
507 wounds were created using a #10 scalpel. Cells were then incubated with the gap junction
508 permeable Lucifer Yellow (420 mw, final concentration 0.05%, Thermo #2790937) and gap
509 junction impermeable Rhodamine Dextran-647 (10,000 mw, final concentration 100 μg/mL
510 ThermoFisher #2860812) for 5 min. Cells were then washed in PBS three times, fixed in 4% PFA
511 for 20 min at room temperature, washed in PBS, and imaged for dye transfer (Nikon A1 confocal).
512 Analysis of dye transfer area for each condition was performed using NI Elements Advanced
513 Research (**Supplemental Figure 12**). Normalized data (to length) was presented as Area/Length
514 of dye transfer.

515 **Western blotting and membrane protein biotinylation and coimmunoprecipitation:** Western
516 blotting, cell surface biotinylation, and co-immunoprecipitation studies were performed as we
517 previously described[24,59]. Proteins for western blotting and cell surface protein biotinylation were
518 harvested in PBS lysis buffer containing 5 mM EDTA, 0.5% sodium deoxycholate, 0.5% NP-40
519 substitute, 1 mM sodium orthovanadate, 10 mM sodium fluoride protease inhibitor cocktail (1:100,
520 Millipore #P8340), phosphatase inhibitor cocktail 2 (1:100, Millipore #P5726), phosphatase
521 inhibitor cocktail 3 (1:100, Sigma #P0044). For co-immunoprecipitation, 10 mM n-
522 ethylmethylamine (Millipore, #291145) was added to the lysis buffer. Protein samples were
523 quantified by BCA assay before loading, and equal loading was confirmed using β-tubulin and

524 total protein assay (Revert 700 Total Protein Stain, LiCor). Membranes were developed using
525 LiCor secondary antibodies, and imaged on a LiCor Odyssey scanner. Expression analysis was
526 performed using Image Studio (LiCor). Values were normalized to total protein stain or β-tubulin,
527 and changes were calculated as a fold change compared to non-treated controls.

528 **Bulk RNA sequencing:** Serum-starved CASMC were plated, stalled for 72 hr, and treated with
529 PDGF-β and peptides overnight. Cells were washed 2x in ice-cold PBS and then lysed in 350 µl
530 of RLT lysis buffer. RNA was harvested (RNeasy Mini Kit, Qiagen #74104) according to the
531 manufacturer's instructions, including the optional DNA removal step. Extracted RNA was
532 quantified using a NanoDrop One spectrophotometer (Thermo Fisher, USA). Aliquots of RNA (1.5
533 µg) were then diluted to equal concentrations (75 ng/µl) in RNase-free water.

534 RNA integrity analysis, library preparation, sequencing, raw read count generation, and
535 differential gene expression analysis were performed commercially by Novogene (Sacremento,
536 CA, USA) using their Human mRNA Sequencing pipeline. Full parameters, protocols, and quality
537 control reports are available on request, but are explained briefly below:

538 RNA integrity was assessed using the 5400 Fragment Analyzer System (Agilent Technologies,
539 CA, USA). mRNA library preparation was performed with poly A enrichment and library quality
540 was verified using Qubit assay for quantification, Agilent Bioanalyzer for size distribution, and
541 qPCR for molarity using adaptor-specific primers. Sequencing was performed on the NovaSeq X
542 Plus (Illumina, USA) platform with 150 bp paired-end reads and a minimum of 6 G raw data. Raw
543 sequencing data in FASTQ format were cleaned using custom in-house (Novogene) Perl scripts.
544 Reads with adapter contamination, reads containing more than 10% uncertain nucleotides, and
545 reads in which more than 50% of bases had a quality (Q) score below 5 were removed. At this
546 point, an outlying sample in the PDGF-β group was removed from all further analysis due to
547 significant AT/GC content separation (**Supplemental Figure 15).** Reads were then aligned to the
548 human genome (hg38) using 'HISAT2' (v2.0.05). Raw read counts were generated using
549 'featureCounts' (v1.5.0-p3). Fragments Per Kilobase of transcript per Million mapped reads
550 (FPKM) was derived from raw data by Novogene and used to calculate Pearson's correlation
551 coefficient to assess intra group and between group variability, and hierarchical clustering.
552 However, for all downstream analysis raw count normalization was performed using 'DESeq2'
553 (v1.44.0) in the R statistical analysis program (v4.4.1). To exclude low count genes prior to
554 'DESeq2' normalization, only genes with at least 10 counts in one sample were kept. Gene
555 symbols were extracted based on provided Ensembl ID using 'clusterProfiler' (v4.12.0) and
556 'org.Hs.eg.db' (v3.19.1). 'DESeq2' normalized counts were $\log_2$ transformed to ensure a normal

557 distribution. Euclidean distances were then calculated and principal component analysis (PCA)
558 was performed using 'dist()' and 'prcomp()', respectively, in base R.

559 Differential gene expression analysis was performed by Novogene for every possible combination
560 of sample groups using 'DESeq2' (v.1.20.0) with Benjamini-Hochberg multiple comparison
561 adjustment. An adjusted p-value (padj) < 0.05 and an $|\log_2(FC)| > 0$ was set as the threshold for
562 differentially expressed genes (DEGs). Volcano plots displaying $-\log_{10}(padj)$ and $\log_2(FC)$ were
563 generated in R.

564 Pathway enrichment analysis was performed on DEGs with a padj < 0.05 with 'clusterProfiler' in
565 R using the Gene Ontology (GO) database. The list of CASMC detected genes after low gene
566 count exclusion was used as the background gene set. The GO terms with a padj < 0.05 following
567 Benjamini-Hochberg multiple comparison adjustment were considered statistically significantly
568 enriched. Separate pathway enrichment analysis was performed for upregulated DEGs ($\log_2(FC)$
569 > 0) and downregulated DEGs ($\log_2(FC) < 0$). Individual GO term heatmaps were generated by
570 extracting 'DESeq2' normalized counts for all DEGs (when comparing PDGF-β+CycliCx to PDGF-
571 β+OT peptide) in indicated statistically significantly enriched pathways and calculating a gene
572 expression z-score for each sample. Data were then visualized using 'pheatmap' (v1.0.12).

573 To interrogate changes in expression of single genes, 'DESeq2' normalized counts were
574 extracted, and the mean normalized counts were plotted in GraphPad Prism 10. A 1-way ANOVA
575 followed by Tukey's multiple comparison testing was performed to assess changes in gene
576 expression between groups. Unless otherwise stated, RNA sequencing data were visualized
577 using 'ggplot2' (v3.5.1). Differential gene analysis and GO pathway analysis data sets are shown
578 in **Supplemental Tables 1-2**.

579 **Statistical analysis:** Statistical analysis was performed using Prism version 10.4.2. Samples
580 were assessed for normal distribution using a Shapiro-Wilk test, and outliers were identified using
581 the Prism robust regression and outlier removal (ROUT) test (Q =1%). 1-way or 2-way multiple
582 comparison ANOVA followed by Dunnett or Tukey's post-test was used for comparisons between
583 >2 groups. The t-test was used for comparisons of 2 treatment groups. Kruskal-Wallis and Mann-
584 Whitney non-parametric tests were used for groups that did not display normal distribution. A
585 minimum of n=3 was used for all statistical analyses, and n values for each experiment are stated
586 in the figure legends. P values are shown for all statistical analyses, with a P value of less than
587 0.05 considered significant. Data represent mean ± SD.

588 **Approval for the use of human excess vascular tissues**

589 The Institutional Review Board (IRB) at Carilion Roanoke Memorial Hospital reviewed and
590 approved the use of de-identified human saphenous vein tissues normally discarded at the end
591 of coronary artery bypass graft surgeries. The Carilion Clinic IRB determined the research does
592 not meet the definition of human subject research as outlined in 45 CFR 46.102(d). Patient data,
593 health data, and identifiable information were not included with specimens.

594 **Data availability**

595 All data generated and used for analysis and original data sets are freely available for further
596 analysis. Bulk RNA sequencing data have been deposited in the Gene Expression Omnibus
597 (GEO) with accession number GSE312484

598 **Author contributions**

599 MCR, MWS, MJ, GSB, BEI, and SRJ designed research studies; MCR, MWS, XL, FI, MRL, KR,
600 RCJ, AM, CLD, AKB, MJ, GSB, and SRJ conducted experiments and acquired data; MCR, MWS,
601 XL, KR, RJ, AM, CLD, GSB, BEI, and SRJ analyzed data; PDL provided reagents; MCR, MWS,
602 BEI, and SRJ wrote the manuscript; All authors approved the final version of the manuscript. A
603 coin flip decided the listed order of co-first authors MCR and MWS; both authors contributed
604 equally.

605 **Acknowledgments**

606 We gratefully acknowledge the resources and services provided Ms. Ruth Macleod at the
607 University of Glasgow for the production of peptide arrays. Servier medical art, licensed under CC
608 BY 4.0 https://creativecommons.org/licenses/by/4.0/, was used to create figure schematics.
609 Funding for this research includes AHA 19CDA34630036 (SJ), AHA 23PRE1010870 (MS), AHA
610 and the DC Women's Board 25POST1410066 (MR), NIH-F31HL170721 (MS), NIH-
611 R215R21HL168614-02 (SJ), VT-Proof of Concept (SJ), and the Seale Innovation Award (SJ).
612 Medical Research Council grant MR/y00364/1 (GSB). NIH HL120840 (BEI), NIH HL137112 (BEI).

613 **References**

614 1. Nedkoff L, Briffa T, Zemedikun D, Herrington S, Wright FL. Global Trends in
615 Atherosclerotic Cardiovascular Disease. *Clin Ther*. Nov 2023;45(11):1087-1091.
616 doi:10.1016/j.clinthera.2023.09.020
617 2. Maron DJ, Hochman JS, Reynolds HR, et al. Initial Invasive or Conservative Strategy for
618 Stable Coronary Disease. *N Engl J Med*. Apr 09 2020;382(15):1395-1407.
619 doi:10.1056/NEJMoa1915922
620 3. Déglise S, Bechelli C, Allagnat F. Vascular smooth muscle cells in intimal hyperplasia, an
621 update. *Front Physiol*. 2022;13:1081881. doi:10.3389/fphys.2022.1081881
622 4. Cornelissen A, Guo L, Fernandez R, et al. Endothelial Recovery in Bare Metal Stents and
623 Drug-Eluting Stents on a Single-Cell Level. *Arterioscler Thromb Vasc Biol*. Aug 2021;41(8):2277-
624 2292. doi:10.1161/ATVBAHA.121.316472
625 5. Bønaa KH, Mannsverk J, Wiseth R, et al. Drug-Eluting or Bare-Metal Stents for Coronary
626 Artery Disease. *N Engl J Med*. Sep 29 2016;375(13):1242-52. doi:10.1056/NEJMoa1607991
627 6. Goodenough DA, Goliger JA, Paul DL. Connexins, connexons, and intercellular
628 communication. *Annu Rev Biochem*. 1996;65:475-502.
629 doi:10.1146/annurev.bi.65.070196.002355
630 7. Gangoso E, Thirant C, Chneiweiss H, Medina JM, Tabernero A. A cell-penetrating peptide
631 based on the interaction between c-Src and connexin43 reverses glioma stem cell phenotype.
632 *Cell Death Dis*. Jan 23 2014;5:e1023. doi:10.1038/cddis.2013.560
633 8. Moorer MC, Hebert C, Tomlinson RE, Iyer SR, Chason M, Stains JP. Defective signaling,
634 osteoblastogenesis and bone remodeling in a mouse model of connexin 43 C-terminal truncation.
635 *J Cell Sci*. Feb 01 2017;130(3):531-540. doi:10.1242/jcs.197285
636 9. Langlois S, Cowan KN, Shao Q, Cowan BJ, Laird DW. The tumor-suppressive function of
637 Connexin43 in keratinocytes is mediated in part via interaction with caveolin-1. *Cancer Res*. May
638 15 2010;70(10):4222-32. doi:10.1158/0008-5472.CAN-09-3281
639 10. Gellhaus A, Dong X, Propson S, et al. Connexin43 interacts with NOV: a possible
640 mechanism for negative regulation of cell growth in choriocarcinoma cells. *J Biol Chem*. Aug 27
641 2004;279(35):36931-42. doi:10.1074/jbc.M404073200
642 11. Fu CT, Bechberger JF, Ozog MA, Perbal B, Naus CC. CCN3 (NOV) interacts with
643 connexin43 in C6 glioma cells: possible mechanism of connexin-mediated growth suppression. *J*
644 *Biol Chem*. Aug 27 2004;279(35):36943-50. doi:10.1074/jbc.M403952200
645 12. Strauss RE, Mezache L, Veeraraghavan R, Gourdie RG. The Cx43 Carboxyl-Terminal
646 Mimetic Peptide αCT1 Protects Endothelial Barrier Function in a ZO1 Binding-Competent
647 Manner. *Biomolecules*. Aug 12 2021;11(8)doi:10.3390/biom11081192
648 13. Smyth JW, Guo S, O'Rourke L, et al. Increased interaction between connexin43 and
649 microtubules is critical for glioblastoma stem-like cell maintenance and tumorigenicity. *bioRxiv*.
650 Jan 27 2024;doi:10.1101/2024.01.26.576347
651 14. Hong T, Hill CE. Restricted expression of the gap junctional protein connexin 43 in the
652 arterial system of the rat. *J Anat*. May 1998;192 (Pt 4)(Pt 4):583-93. doi:10.1046/j.1469-
653 7580.1998.19240583.x
654 15. Liao Y, Regan CP, Manabe I, et al. Smooth muscle-targeted knockout of connexin43
655 enhances neointimal formation in response to vascular injury. *Arterioscler Thromb Vasc Biol*. May
656 2007;27(5):1037-42. doi:10.1161/ATVBAHA.106.137182
657 16. Chadjichristos CE, Matter CM, Roth I, et al. Reduced connexin43 expression limits
658 neointima formation after balloon distension injury in hypercholesterolemic mice. *Circulation*. Jun
659 20 2006;113(24):2835-43. doi:10.1161/CIRCULATIONAHA.106.627703
660 17. Zhang A, Han Y, Wang B, Li S, Gan W. Beyond Gap Junction Channel Function: the
661 Expression of Cx43 Contributes to Aldosterone-Induced Mesangial Cell Proliferation via the
662 ERK1/2 and PKC Pathways. *Cell Physiol Biochem*. 2015;36(3):1210-22. doi:10.1159/000430291

663 18. Tittarelli A, Guerrero I, Tempio F, et al. Overexpression of connexin 43 reduces melanoma
664 proliferative and metastatic capacity. *Br J Cancer*. Jul 14 2015;113(2):259-67.
665 doi:10.1038/bjc.2015.162
666 19. Arshad M, Conzelmann C, Riaz MA, Noll T, Gündüz D. Inhibition of Cx43 attenuates
667 ERK1/2 activation, enhances the expression of Cav-1 and suppresses cell proliferation. *Int J Mol*
668 *Med*. Nov 2018;42(5):2811-2818. doi:10.3892/ijmm.2018.3828
669 20. Chadjichristos CE, Morel S, Derouette JP, et al. Targeting connexin 43 prevents platelet-
670 derived growth factor-BB-induced phenotypic change in porcine coronary artery smooth muscle
671 cells. *Circ Res*. Mar 28 2008;102(6):653-60. doi:10.1161/CIRCRESAHA.107.170472
672 21. Plenz G, Ko YS, Yeh HI, et al. Upregulation of connexin43 gap junctions between
673 neointimal smooth muscle cells. *Eur J Cell Biol*. Oct 2004;83(10):521-30. doi:10.1078/0171-9335-
674 00417
675 22. Yeh HI, Lupu F, Dupont E, Severs NJ. Upregulation of connexin43 gap junctions between
676 smooth muscle cells after balloon catheter injury in the rat carotid artery. *Arterioscler Thromb*
677 *Vasc Biol*. Nov 1997;17(11):3174-84. doi:10.1161/01.atv.17.11.3174
678 23. Sorgen PL, Duffy HS, Sahoo P, Coombs W, Delmar M, Spray DC. Structural changes in
679 the carboxyl terminus of the gap junction protein connexin43 indicates signaling between binding
680 domains for c-Src and zonula occludens-1. *J Biol Chem*. Dec 24 2004;279(52):54695-701.
681 doi:10.1074/jbc.M409552200
682 24. Johnstone SR, Kroncke BM, Straub AC, et al. MAPK phosphorylation of connexin 43
683 promotes binding of cyclin E and smooth muscle cell proliferation. *Circ Res*. Jul 6
684 2012;111(2):201-11. doi:10.1161/circresaha.112.272302
685 25. González-Sánchez A, Jaraíz-Rodríguez M, Domínguez-Prieto M, Herrero-González S,
686 Medina JM, Tabernero A. Connexin43 recruits PTEN and Csk to inhibit c-Src activity in glioma
687 cells and astrocytes. *Oncotarget*. Aug 02 2016;7(31):49819-49833.
688 doi:10.18632/oncotarget.10454
689 26. Solan JL, Marquez-Rosado L, Sorgen PL, Thornton PJ, Gafken PR, Lampe PD.
690 Phosphorylation at S365 is a gatekeeper event that changes the structure of Cx43 and prevents
691 down-regulation by PKC. *J Cell Biol*. Dec 17 2007;179(6):1301-9. doi:10.1083/jcb.200707060
692 27. Ohtsubo M, Theodoras AM, Schumacher J, Roberts JM, Pagano M. Human cyclin E, a
693 nuclear protein essential for the G1-to-S phase transition. *Mol Cell Biol*. May 1995;15(5):2612-24.
694 doi:10.1128/MCB.15.5.2612
695 28. George SJ, Wan S, Hu J, MacDonald R, Johnson JL, Baker AH. Sustained reduction of
696 vein graft neointima formation by ex vivo TIMP-3 gene therapy. *Circulation*. Sep 13 2011;124(11
697 Suppl):S135-42. doi:10.1161/CIRCULATIONAHA.110.012732
698 29. George SJ, Williams A, Newby AC. An essential role for platelet-derived growth factor in
699 neointima formation in human saphenous vein in vitro. *Atherosclerosis*. Feb 1996;120(1-2):227-
700 40. doi:10.1016/0021-9150(95)05717-x
701 30. Saxton RA, Sabatini DM. mTOR Signaling in Growth, Metabolism, and Disease. *Cell*. Mar
702 09 2017;168(6):960-976. doi:10.1016/j.cell.2017.02.004
703 31. Sedovy MW, Leng X, Iqbal F, et al. Preserving Endothelial Integrity in Human Saphenous
704 Veins during Preparation for Coronary Bypass Surgery. *J Vasc Res*. Jan 12 2024:1-9.
705 doi:10.1159/000535843
706 32. O'Sullivan M, Scott SD, McCarthy N, et al. Differential cyclin E expression in human in-
707 stent stenosis smooth muscle cells identifies targets for selective anti-restenosis therapy.
708 *Cardiovasc Res*. Dec 01 2003;60(3):673-83. doi:10.1016/j.cardiores.2003.09.018
709 33. Rhett JM, Calder BW, Fann SA, Bainbridge H, Gourdie RG, Yost MJ. Mechanism of action
710 of the anti-inflammatory connexin43 mimetic peptide JM2. *Am J Physiol Cell Physiol*. Sep 01
711 2017;313(3):C314-C326. doi:10.1152/ajpcell.00229.2016

712 34. Calder BW, Matthew Rhett J, Bainbridge H, Fann SA, Gourdie RG, Yost MJ. Inhibition of
713 connexin 43 hemichannel-mediated ATP release attenuates early inflammation during the foreign
714 body response. *Tissue Eng Part A*. Jun 2015;21(11-12):1752-62. doi:10.1089/ten.TEA.2014.0651
715 35. He D, Ma Z, Xue K, Li H. Juxtamembrane 2 mimic peptide competitively inhibits
716 mitochondrial trafficking and activates ROS-mediated apoptosis pathway to exert anti-tumor
717 effects. *Cell Death Dis*. Mar 24 2022;13(3):264. doi:10.1038/s41419-022-04639-6
718 36. Lampe PD, Kurata WE, Warn-Cramer BJ, Lau AF. Formation of a distinct connexin43
719 phosphoisoform in mitotic cells is dependent upon p34cdc2 kinase. *J Cell Sci*. Mar 1998;111 (Pt
720 6):833-41. doi:10.1242/jcs.111.6.833
721 37. Kanemitsu MY, Jiang W, Eckhart W. Cdc2-mediated phosphorylation of the gap junction
722 protein, connexin43, during mitosis. *Cell Growth Differ*. Jan 1998;9(1):13-21.
723 38. Cameron SJ, Malik S, Akaike M, et al. Regulation of epidermal growth factor-induced
724 connexin 43 gap junction communication by big mitogen-activated protein kinase1/ERK5 but not
725 ERK1/2 kinase activation. *J Biol Chem*. May 16 2003;278(20):18682-8.
726 doi:10.1074/jbc.M213283200
727 39. Doble BW, Dang X, Ping P, et al. Phosphorylation of serine 262 in the gap junction protein
728 connexin-43 regulates DNA synthesis in cell-cell contact forming cardiomyocytes. *J Cell Sci*. Jan
729 26 2004;117(Pt 3):507-14. doi:10.1242/jcs.00889
730 40. Jaraíz-Rodríguez M, Talaverón R, García-Vicente L, et al. Connexin43 peptide, TAT-
731 Cx43266-283, selectively targets glioma cells, impairs malignant growth, and enhances survival
732 in mouse models in vivo. *Neuro Oncol*. Apr 15 2020;22(4):493-504. doi:10.1093/neuonc/noz243
733 41. Jiang J, Hoagland D, Palatinus JA, et al. Interaction of α Carboxyl Terminus 1 Peptide
734 With the Connexin 43 Carboxyl Terminus Preserves Left Ventricular Function After Ischemia-
735 Reperfusion Injury. *J Am Heart Assoc*. Aug 20 2019;8(16):e012385.
736 doi:10.1161/JAHA.119.012385
737 42. King DR, Sedovy MW, Leng X, et al. Mechanisms of Connexin Regulating Peptides.
738 *International Journal of Molecular Sciences*. 2021;22(19)doi:10.3390/ijms
739 43. Jackman M, Kubota Y, den Elzen N, Hagting A, Pines J. Cyclin A- and cyclin E-Cdk
740 complexes shuttle between the nucleus and the cytoplasm. *Mol Biol Cell*. Mar 2002;13(3):1030-
741 45. doi:10.1091/mbc.01-07-0361
742 44. Moore JD, Yang J, Truant R, Kornbluth S. Nuclear import of Cdk/cyclin complexes:
743 identification of distinct mechanisms for import of Cdk2/cyclin E and Cdc2/cyclin B1. *J Cell Biol*.
744 Jan 25 1999;144(2):213-24. doi:10.1083/jcb.144.2.213
745 45. Gaulin JF, Fiset A, Fortier S, Faure RL. Characterization of Cdk2-cyclin E complexes in
746 plasma membrane and endosomes of liver parenchyma. Insulin-dependent regulation. *J Biol*
747 *Chem*. Jun 02 2000;275(22):16658-65. doi:10.1074/jbc.275.22.16658
748 46. Akiyama T, Ohuchi T, Sumida S, Matsumoto K, Toyoshima K. Phosphorylation of the
749 retinoblastoma protein by cdk2. *Proc Natl Acad Sci U S A*. Sep 01 1992;89(17):7900-4.
750 doi:10.1073/pnas.89.17.7900
751 47. O'Quinn MP, Palatinus JA, Harris BS, Hewett KW, Gourdie RG. A peptide mimetic of the
752 connexin43 carboxyl terminus reduces gap junction remodeling and induced arrhythmia following
753 ventricular injury. Research Support, N.I.H., Extramural Research Support, Non-U.S. Gov't.
754 *Circulation Research*. Mar 18 2011;108(6):704-15. doi:10.1161/circresaha.110.235747
755 48. Rhett JM, Jourdan J, Gourdie RG. Connexin 43 connexon to gap junction transition is
756 regulated by zonula occludens-1. *Mol Biol Cell*. May 2011;22(9):1516-28. doi:10.1091/mbc.E10-
757 06-0548
758 49. Ek-Vitorin JF, King TJ, Heyman NS, Lampe PD, Burt JM. Selectivity of connexin 43
759 channels is regulated through protein kinase C-dependent phosphorylation. *Circ Res*. Jun 23
760 2006;98(12):1498-505. doi:10.1161/01.RES.0000227572.45891.2c

761 50. Lampe PD, TenBroek EM, Burt JM, Kurata WE, Johnson RG, Lau AF. Phosphorylation of
762 connexin43 on serine368 by protein kinase C regulates gap junctional communication. *J Cell Biol*.
763 Jun 26 2000;149(7):1503-12. doi:10.1083/jcb.149.7.1503
764 51. Gaudino M, Benedetto U, Fremes S, et al. Radial-Artery or Saphenous-Vein Grafts in
765 Coronary-Artery Bypass Surgery. *N Engl J Med*. May 31 2018;378(22):2069-2077.
766 doi:10.1056/NEJMoa1716026
767 52. van der Meer J, Hillege HL, van Gilst WH, et al. A comparison of internal mammary artery
768 and saphenous vein grafts after coronary artery bypass surgery. No difference in 1-year occlusion
769 rates and clinical outcome. CABADAS Research Group of the Interuniversity Cardiology Institute
770 of The Netherlands. *Circulation*. Nov 1994;90(5):2367-74. doi:10.1161/01.cir.90.5.2367
771 53. Tector AJ, Schmahl TM, Janson B, Kallies JR, Johnson G. The internal mammary artery
772 graft. Its longevity after coronary bypass. *JAMA*. Nov 13 1981;246(19):2181-3.
773 54. Gaudino M, Bakaeen FG, Sandner S, et al. Expert Systematic Review on the Choice of
774 Conduits for Coronary Artery Bypass Grafting: Endorsed by the European Association for Cardio-
775 Thoracic Surgery (EACTS) and The Society of Thoracic Surgeons (STS). *Ann Thorac Surg*. Oct
776 2023;116(4):659-674. doi:10.1016/j.athoracsur.2023.06.010
777 55. Bonacquisti EE, Nguyen J. Connexin 43 (Cx43) in cancer: Implications for therapeutic
778 approaches via gap junctions. *Cancer Lett*. Feb 01 2019;442:439-444.
779 doi:10.1016/j.canlet.2018.10.043
780 56. Bolger GB, Baillie GS, Li X, et al. Scanning peptide array analyses identify overlapping
781 binding sites for the signalling scaffold proteins, beta-arrestin and RACK1, in cAMP-specific
782 phosphodiesterase PDE4D5. *Biochem J*. Aug 15 2006;398(1):23-36. doi:10.1042/BJ20060423
783 57. Futaki S, Ohashi W, Suzuki T, et al. Stearylated arginine-rich peptides: a new class of
784 transfection systems. *Bioconjug Chem*. Nov-Dec 2001;12(6):1005-11. doi:10.1021/bc015508l
785 58. Johnstone SR, Ross J, Rizzo MJ, et al. Oxidized phospholipid species promote in vivo
786 differential cx43 phosphorylation and vascular smooth muscle cell proliferation. *Am J Pathol*. Aug
787 2009;175(2):916-24. doi:ajpath.2009.090160 [pii]
788 10.2353/ajpath.2009.090160
789 59. Yang Y, Delalio LJ, Best AK, et al. Endothelial Pannexin 1 Channels Control Inflammation
790 by Regulating Intracellular Calcium. *J Immunol*. Jun 2020;204(11):2995-3007.
791 doi:10.4049/jimmunol.1901089

Figure 1: PDGF-β induces new intima in human saphenous veins in vitro, associated with an increase in Cx43 and proliferation markers

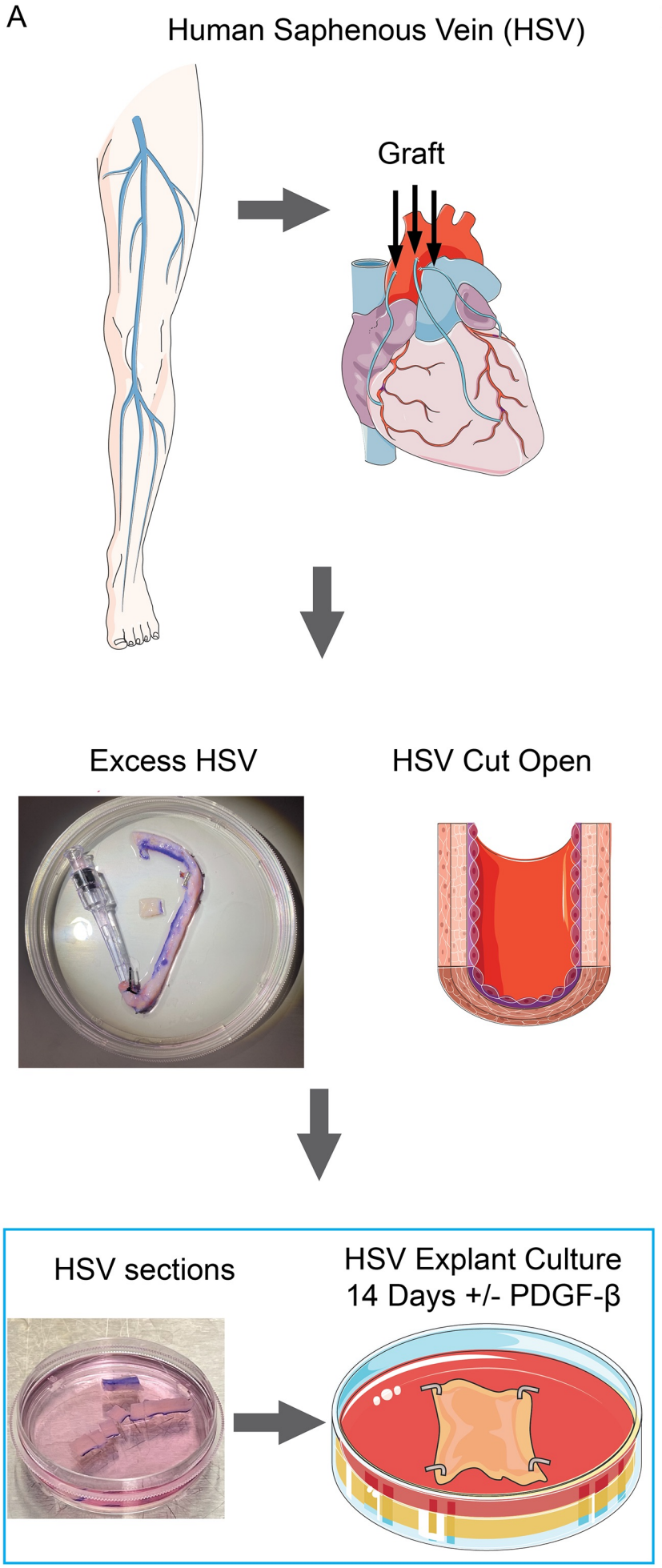

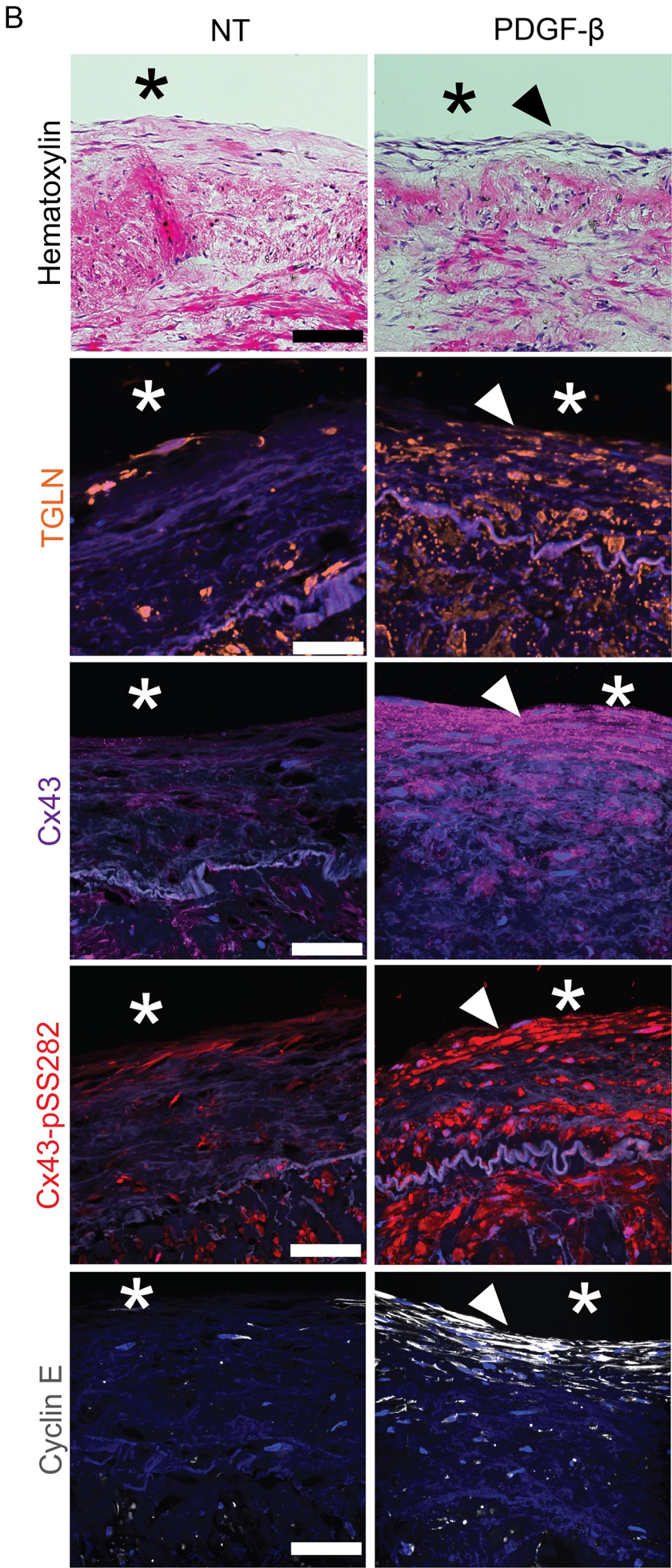

Figure 2: Design of the CycliCx peptide using peptide arrays demonstrates cyclin E binding regions on the phosphorylated Cx43CT

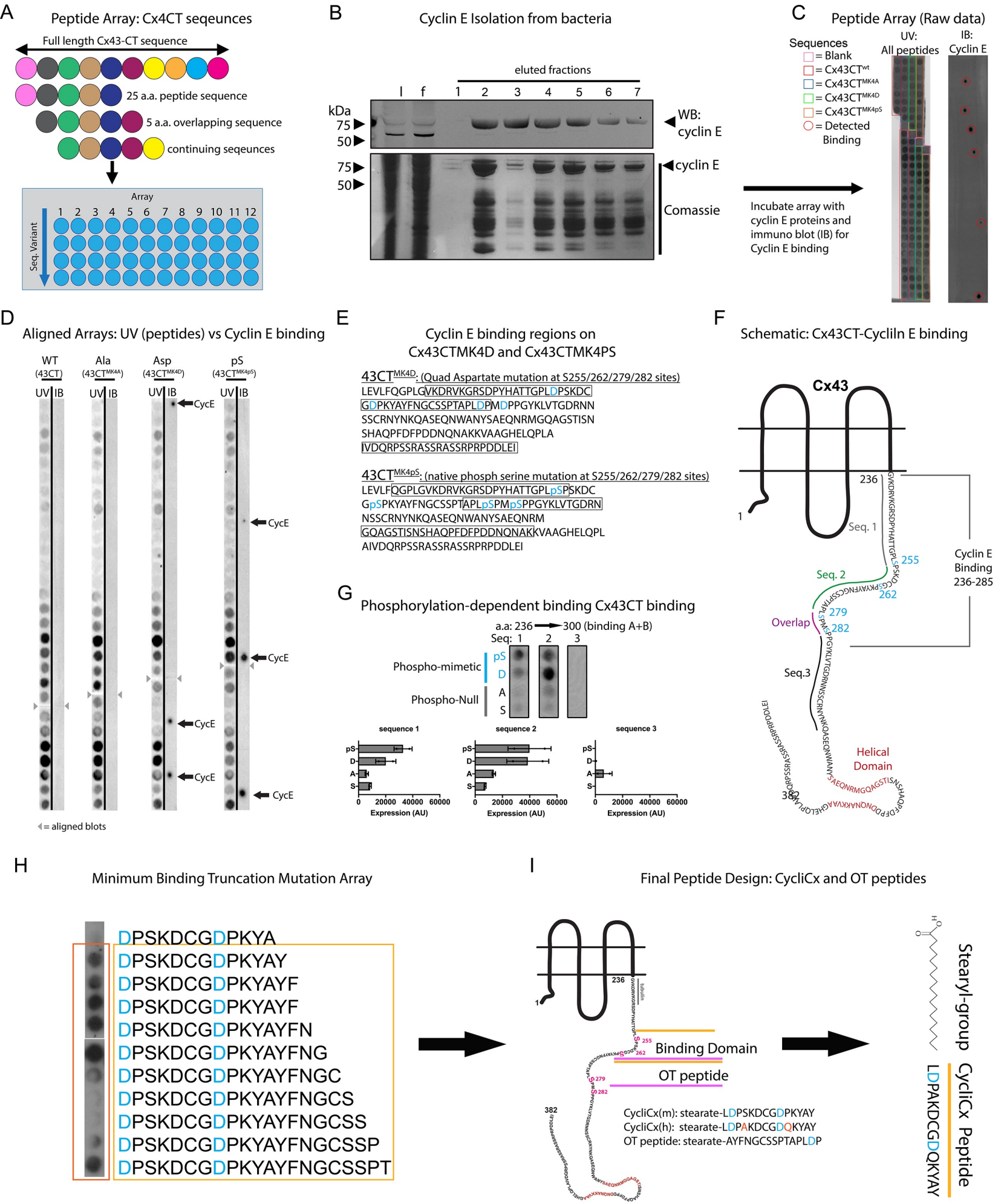

Figure 3: CycliCx Peptide alters Cx43 expression and interactions with cyclin E

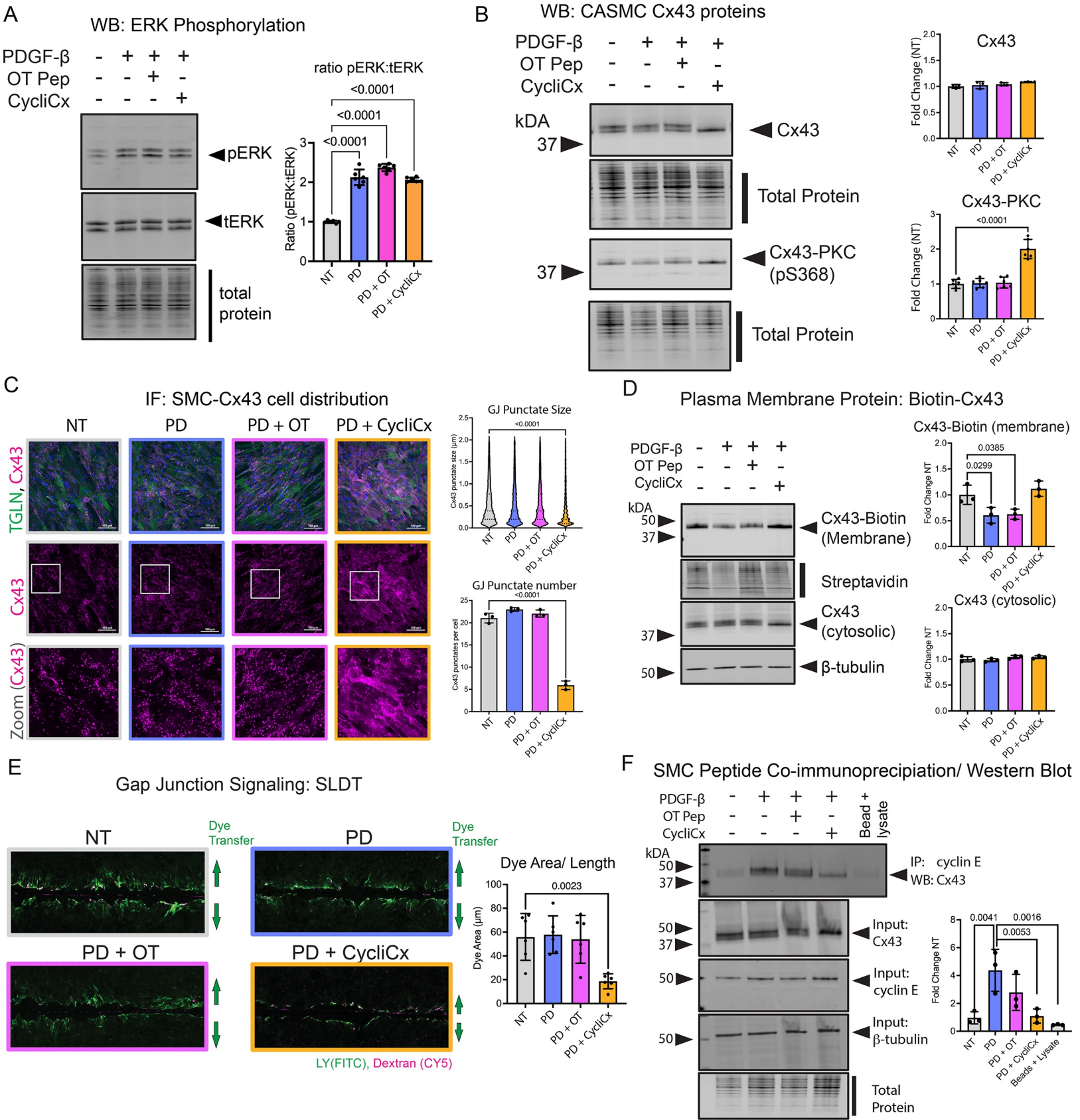

Figure 4: Transcriptomics reveals that the CycliCx peptide arrests cell cycle progression at G1/S phase transition

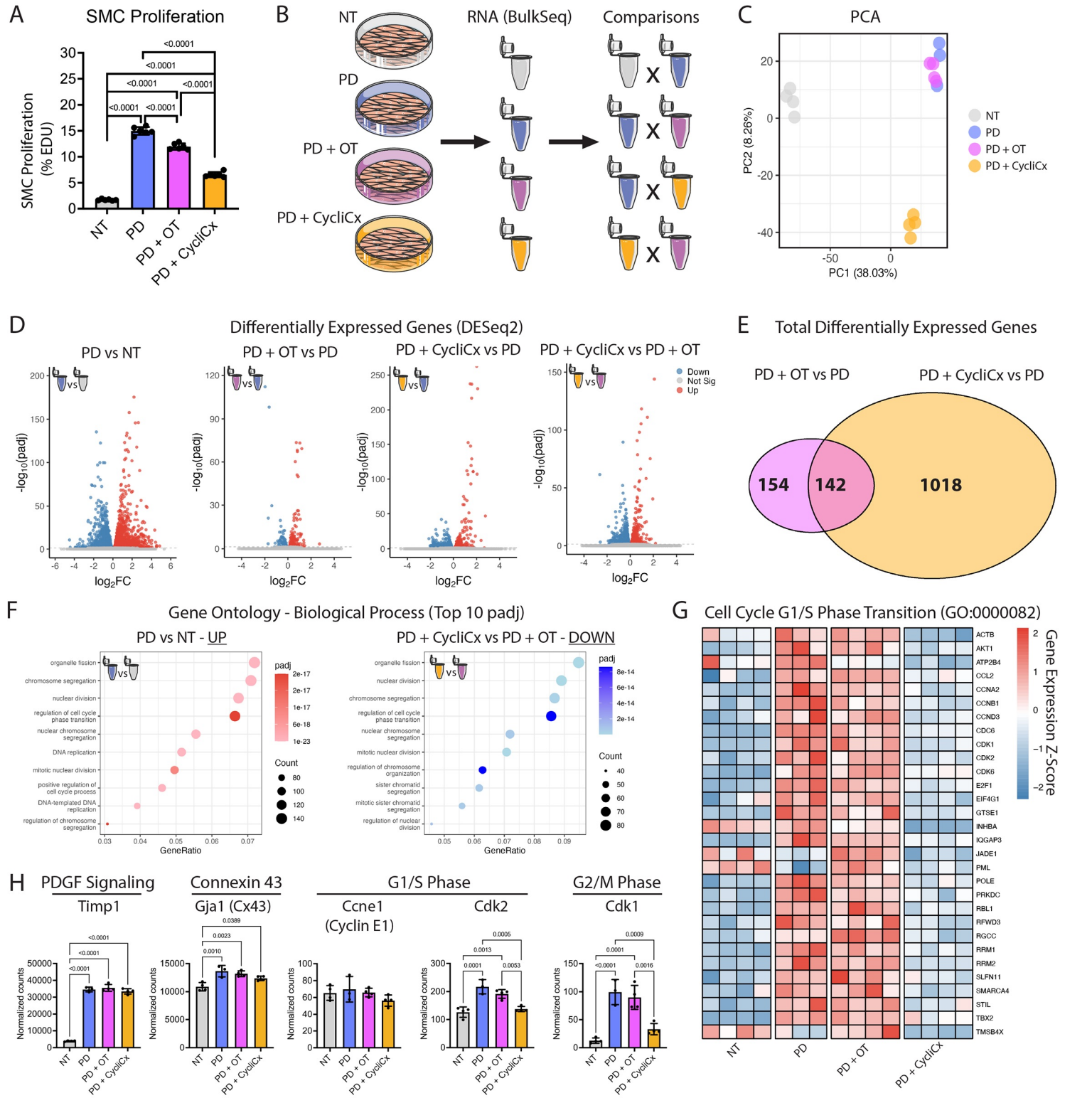
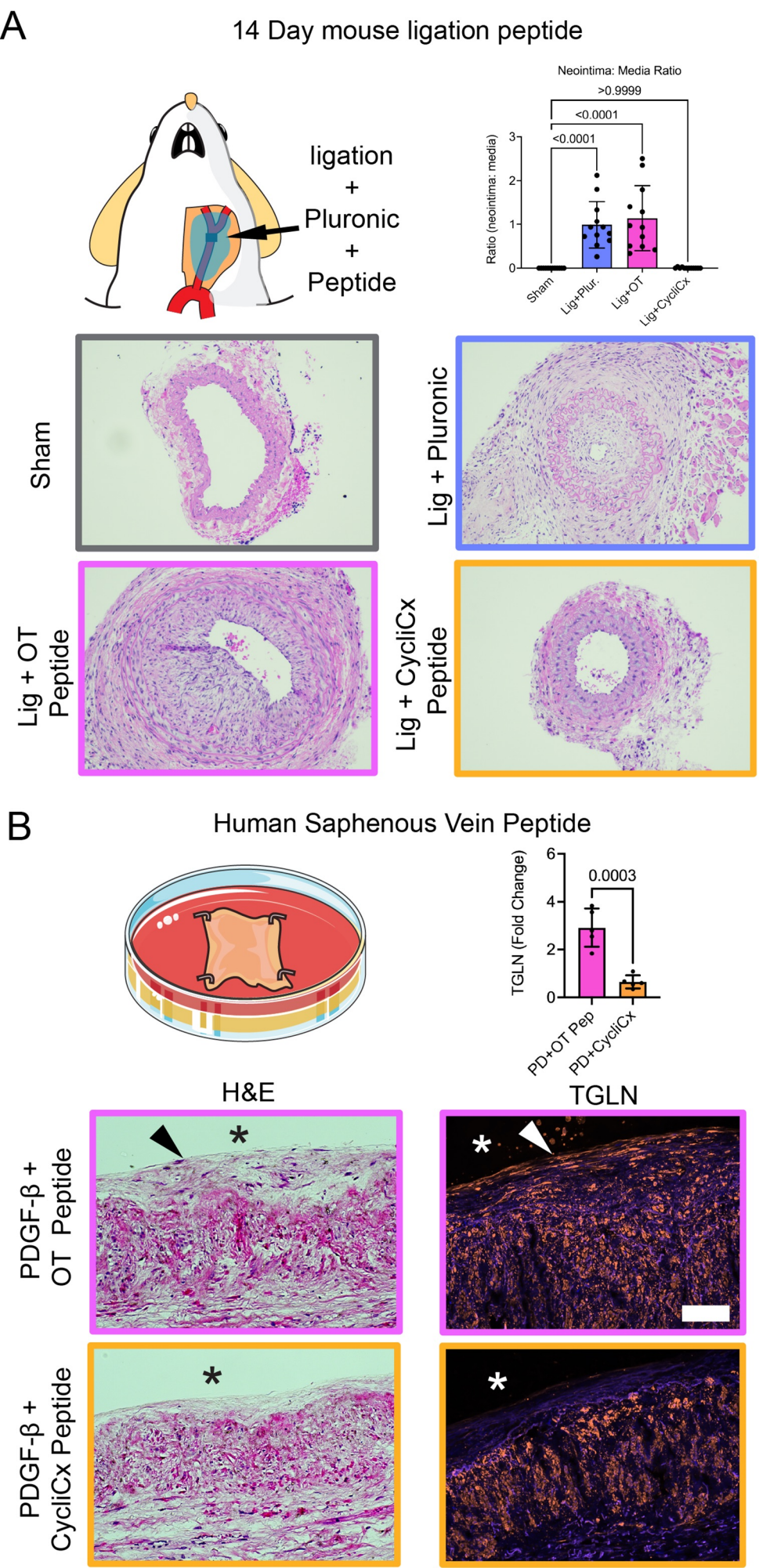
Figure 5: CycliCx peptide limits neointima formation in mouse and human blood vessels